ITERATIVE INTERFERENCE CANCELLATION AND DECODING FOR SPREAD-SIGNATURE CDMA SYSTEMS

Soosan Beheshti and Gregory W. Wornell

Research Laboratory of Electronics
Massachusetts Institute of Technology
Cambridge, MA 02139 USA

Abstract — Spread-signature code-division multiple-access systems are designed to allow both time and frequency diversity to be exploited in multiuser wireless systems operating in fading environments. Computationally efficient multipass demodulation and decoding algorithms are developed for use in receivers with these systems. These algorithms efficiently suppress both intersymbol and interuser (multiple-access) interference to achieve a substantial diversity benefit and good near-far resistance characteristics. Moreover, it is shown that relatively few iterations are required for convergence to typical target bit-error rates. Several other aspects of the performance of the algorithms are also explored.

I. INTRODUCTION

Spread-signature code-division multiple-access (CDMA) systems were recently introduced as an attractive alternative to conventional CDMA systems for use in time-varying multipath environments [1] [2]. Using long signatures in an overlapped manner for successive symbols, spread-signature CDMA can achieve a substantial temporal diversity benefit. Furthermore, the broadband nature of the signatures allows an additional spectral diversity benefit to be simultaneously realized.

In [1], computationally very efficient linear receivers were developed for use in conjunction with spread-signature CDMA. With such receivers, it was shown that spread-signature CDMA effectively transforms the multiuser Rayleigh fading channel into a decoupled set of additive white quasi-Gaussian noise channels. In particular, both the intersymbol and interuser (i.e., multiple-access) interferences are transformed into a second quasi-Gaussian noise source that is effectively white and uncorrelated with the input data stream.

Improved performance can be obtained by more carefully exploiting the digital (finite alphabet) nature of the users' data streams, which makes the intersymbol and interuser interferences highly structured. In principle, direct maximum likelihood (ML) decoding algorithms can be employed for optimum mitigation of such interference at the receiver. However, the associated Viterbi algorithms are invariably impractical, even for conventional CDMA systems. Indeed, ML interuser interference cancellation has complexity that grows exponentially with the number of users [3]. Moreover, ML intersymbol interference cancellation is often computationally unwieldy even for single-user systems [4].

This work has been supported in part by DARPA monitored by ONR under Contract No. N00014-93-1-0686, the Office of Naval Research under Grant No. N00014-96-1-0930, the National Science Foundation under Grant No. MIP-9502885, and Army Research Laboratory under Cooperative Agreement DAAL01-96-2-0002.

In this paper, we describe efficient techniques for suppressing such interference at the receiver during demodulation and decoding. These algorithms explicitly take into account the structure in the interference and result in a near-far resistant receiver, but avoid the cumbersome complexity of ML decoding. In single-user scenarios, spread-signature CDMA specializes to the class of spread-response precoding algorithms described in [2]. In this case the interference suppression algorithms developed in this paper specialize to an efficient variant of the novel multistage receivers described by Wittneben in [5], for which useful new insights are obtained.

II. SYSTEM MODEL

We consider a single cell of a typical cellular multiple-access channel in which there is a single base station and M mobiles. Both forward link (base-to-mobile) and reverse link (mobile-to-base) communication are of interest, and the users share a total fixed bandwidth of MW_0, where W_0 is the bandwidth per user. The information to be sent by the mth user is a white N-PSK stream of (possibly coded) symbols $x_m[n]$, each with energy $\mathcal{E}_m$. The discrete-time transmission $y_m[n]$ for the mth user is obtained by upsamping $x_m[n]$ by a factor of M, followed by linear time-invariant filtering with the associated signature sequence $h_m[n]$, i.e.,

$$y_m[n] = \sum_k x_m[k]\, h_m[n - kM], \tag{1}$$

The signatures $h_m[n]$ form an orthonormal set, i.e.,

$$\sum_k h_i[k - nM]\, h_l[k - mM] = \delta[n - m]\, \delta[i - l], \tag{2}$$

so that all the symbols of all the users are modulated on orthogonal, unit-energy waveforms. In spread-signature systems, these signatures have the further property that their length K is much larger than the intersymbol period M. Choosing larger spreading factors K allows larger temporal diversity benefits to be achieved. While much of our development applies more broadly, in experiments we use the so-called maximally-spread signatures [1], which are binary valued ($h_m[n] = \pm K^{-1/2}$) and particularly attractive for practical implementations.

The multiuser channel is a time- and frequency-selective Rayleigh fading with stationary, uncorrelated scattering. In the equivalent discrete-time baseband model, the signal obtained at a particular receiver takes the form

$$r[n] = \sum_m \sum_k a_m[n; k]\, y_m[n - k] + w[n], \tag{3}$$

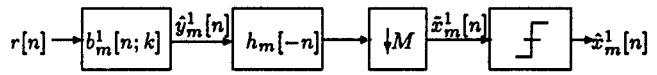

Fig. 1. First pass of iterative decoding.

where $a_m[n;k]$ denotes the zero-mean, ergodic, complex-valued, circularly-symmetric Gaussian kernel of the random, linear time-varying system modeling the fading process encountered by the mth user, and $w[n]$ is zero-mean, complex-valued, circularly symmetric, stationary white Gaussian receiver noise. The time-varying frequency response of the channel is $A_m(\omega;n] = \sum_k a_m[n;k]\, e^{-j\omega}$, and $\operatorname{var} A_m(\omega;n] = \sigma_m^2$, while the noise $w[n]$ has variance $\operatorname{var} w[n] = \mathcal{N}_0\mathcal{W}_0$. We assume the receiver has perfect knowledge of the $a_m[n;k]$, though in practice these quantities must be estimated either blindly or through the use of training data.

III. MULTIPASS RECEIVERS

The demodulation/decoding algorithm we develop in this section is a batch iterative algorithm involving successive processing of the received data stream. In describing the algorithm, we denote the parameters associated with the processing at the lth iteration using a superscript l.

A. *First Pass ($l = 1$)*

To decode the mth user's symbol stream, the observed data $r[n]$ is first processed by the linear receiver described in [1] and depicted in Fig. 1. First, the data is filtered with a linear time-varying equalizer with kernel $b_m^1[n;k]$. The second step is signature demodulation by correlation and downsampling. The equalizer is chosen so as to maximize the signal-to-noise+interference ratio (SNIR) after this second step. Finally, the symbols are recovered by passing the demodulated data through a suitably designed slicer.

The demodulated stream can be expressed as

$$\tilde{x}_m^1[n] = \mu_{mm}^1\, x[n] + v_m[n] \tag{4}$$

where

$$v_m[n] = u_m^1[n] + z_{mm}^1 + \sum_{i\neq m} z_{im}^1[n]. \tag{5}$$

In (5), $u_m^1[n]$ is the component due to the noise and has variance $\mathcal{N}_0\mathcal{W}_0 E\left[|B_m^1|^2\right]$, where $B_m^1(w;n] = \sum_k b_m^1[n;k]\, e^{-j\omega k}$. The component $z_{im}^1[n]$ is the interference due to the ith user, and can be expressed in the form

$$z_{im}^1[n] = \sum_k t_{im}^1[k]\, x_i[k]. \tag{6}$$

In (6), where $t_{im}^1[n]$ is a zero-mean function of both $h_i[n]$ and the kernel of the system formed from cascading the channel $a_i[n;k]$ and the equalizer $b_m^1[n;k]$, i.e.,

$$c_{im}^1[n;k] = \sum_l b_m^1[n;l]\, a_i[n-l;k-l]. \tag{7}$$

As such, $z_{mm}^1[n]$ represents the intersymbol interference and the remaining $z_{im}^1[n]$ are multiple-access interference terms. Each of the interference terms has variance $(\mathcal{E}_i/M)\operatorname{var} C_{im}^1(w;n]$, where $C_{im}^1(\omega;n] = \sum_k c_{im}^1\, e^{-j\omega k}$, and $E\left[C_{mi}^1(\omega;n]\right] = \mu_{mm}^1\,\delta[m-i]$.

When sufficiently long signatures are used, the symbol stream $x_m[n]$ is uncorrelated not only with the noise and multiple-access interference terms, but with the intersymbol interference term as well [1]. In this case, the SNIR

$$\gamma_m^1(B_m^1) = \frac{|\mu_m^1|^2\mathcal{E}_m}{\mathcal{N}_0\mathcal{W}_0 E[|B_m^1|^2] + \frac{1}{M}\sum_{i=1}^M \mathcal{E}_i \operatorname{var} C_{im}^1}. \tag{8}$$

fully describes the second-order characteristics of the system up to the slicer of the first decoding pass. Moreover, in the long-signature scenario, the resulting quasi-Gaussian characteristics of the interference means that the symbol error rate performance of the symbol-by-symbol threshold detector for the N-PSK stream $x_m[n]$ can be approximated by [6]

$$\Pr(\varepsilon_m) = 2\mathcal{Q}\left(\sin\left(\frac{\pi}{N}\right)\sqrt{2\gamma_m^1}\right), \tag{9}$$

where $\mathcal{Q}(v) = \frac{1}{\sqrt{2\pi}}\int_v^\infty e^{-v^2/2}\, dv$.

B. *Subsequent Passes*

The decoding described above achieves a substantial improvement in average bit-error rate performance over conventional CDMA systems by exploiting temporal diversity via linear processing and taking into account the second-order characteristics of the received signal. However, because the interference is effectively treated as if it were white Gaussian noise, the resulting system is interference-limited—the bit-error rate does not go to zero with increasing SNR—making it vulnerable to near-far effects [3].

By exploiting higher-order statistics of the interference in the received signal, its effects can be more effectively mitigated. As we now describe, this is accomplished using a multipass estimator-canceler structure for interference suppression that is somewhat analogous to that used in minimum mean-square error decision-feedback equalizers [7]. In particular, using the receiver just described we obtain preliminary estimates $\hat{x}_m^1[n]$ for each of the M different symbol streams at the receiver. In turn, using these estimates together with the fading channel kernels in conjunction with (6), we generate refined estimates $\hat{z}_{im}^1[n]$ of the interference terms in (5). These estimates can be effectively subtracted from an appropriately equalized and demodulated version of the data $\tilde{x}_m^1[n]$, allowing more reliable symbol estimates $\hat{x}_m^2[n]$ to be obtained from the slicer. This process is then repeated, exploiting the estimates $\hat{x}_m^2[n]$ to generate further refined interference estimates $\hat{z}_{im}^2[n]$, etc. We now develop the details of this strategy.

The interference estimator for the lth pass takes the form depicted in Fig. 2. In the upper path, the estimated symbol is re-modulated on its signature, processed by a noise-free replica of the channel, then demodulated by a replica of the receiver with a linear equalizer $b_m^l[n;k]$ whose time-varying frequency response we denote by $B_m^l(\omega;n]$. The cascade of this equalizer with the channel corresponding to $a_i[n;k]$ has kernel

$$c_{im}^l[n;k] = \sum_j b_m^l[n;j]\, a_i[n-j;k-j], \tag{10}$$

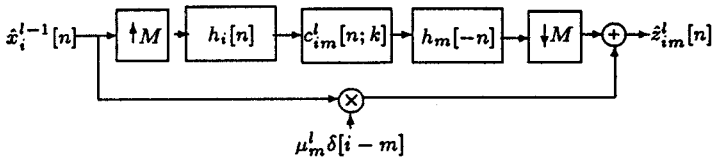

Fig. 2. Interference estimation for the lth decoding pass.

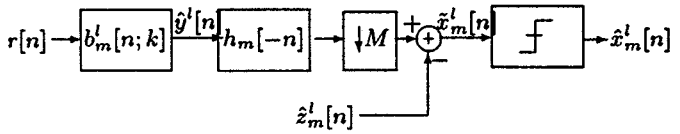

Fig. 3. Interference cancellation in the lth pass of decoding.

and the associated time-varying frequency response has mean $E\left[C_{im}^l[n;k]\right] = \mu_{mm}^l \delta[m-i]$. Note that the lower path in Fig. 2 is required for intersymbol but not interuser interference estimation. The resulting interference estimate can be expressed in the form

$$\hat{z}_{im}^l[n] = \sum_k t_{im}^l[k]\, \hat{x}_i^{l-1}[k], \tag{11}$$

where $t_{im}^l[n]$ is a zero-mean function of $h_i[n]$ and $c_{im}^l[n;k]$.

The associated interference canceler in the lth pass takes the form depicted in Fig. 3. In particular, we subtract a linear combination of the estimated interferences, i.e.,

$$\hat{z}_m^l[n] = \sum_i \alpha_{im}^l\, \hat{z}_{im}^l[n]. \tag{12}$$

In general, we seek equalizer coefficients $b_m^l[n;k]$ and canceler weights α_{im}^l so as to obtain the smallest possible symbol error rate at the output $\hat{x}_m^l[n]$ of the slicer. The slicer input takes the form

$$\tilde{x}_m^l[n] = \mu_m^l\, x_m[n] + v_m^l[n] \tag{13}$$

where

$$v_m^l[n] = u_m^l[n] + \sum_i \tilde{z}_{im}^l[n] \tag{14}$$

with

$$\tilde{z}_{im}^l[n] = z_{im}^l[n] - \alpha_{im}^l\, \hat{z}_{im}^l[n]. \tag{15}$$

and [cf. (11)]

$$z_{im}^l[n] = \sum_k t_{im}^l[k]\, x_i[k]. \tag{16}$$

When the correlation between $v_m^l[n]$ and $x_m[n]$ is small, the symbol error probability can be approximated in a manner analogous to that used to obtain (9), yielding

$$\Pr(\varepsilon_m^l) = 2Q\left(\sin\left(\frac{\pi}{N}\right)\sqrt{2\gamma_m^l}\right), \tag{17}$$

where

$$\gamma_m^l = \frac{\mathcal{E}_m |\mu_m^l|^2}{\operatorname{var} v_m^l}. \tag{18}$$

is the new SNIR we seek to maximize.

To maximize the SNIR over the weights α_{im}^l, it suffices to minimize the interference power. First, note that at high SNR we have

$$\operatorname{var} \hat{z}_{im}^l \approx \operatorname{var} z_{im}^l = (\mathcal{E}_i/M) \operatorname{var} C_{im}^l, \tag{19}$$

and that the normalized correlation between the actual and estimated symbols takes the form

$$\frac{E\left[x_i[n]\cdot \hat{x}_i^l[k]\right]}{\sqrt{\operatorname{var} x_i[n]}\sqrt{\operatorname{var} \hat{x}_i[k]}} \approx \rho_i^l\, \delta[n-k], \tag{20}$$

so that using (11) and (16) in (15), we obtain

$$\operatorname{var} \tilde{z}_{im}^l[n] \approx \left[1 + (\alpha_{im}^l)^2 - 2\alpha_{im}^l \rho_i^{l-1}\right] \frac{\mathcal{E}_i}{M} \operatorname{var}[C_{im}^l]. \tag{21}$$

It is then straightforward to verify that (21) achieves its minimum value $\sum_i (1-(\rho_i^{l-1})^2)(\mathcal{E}_i/M) \operatorname{var}[C_{im}^l]$ when we choose $\alpha_{im}^l = \rho_i^{l-1}$.

Hence, in terms of the optimized weights the SNIR (18) in the lth pass can be expressed in the form

$$\gamma_m^l(B_m^l) = \frac{|\mu_m^l|^2 \mathcal{E}_m}{\mathcal{N}_0 \mathcal{W}_0 E[|B_m^l|^2] + \frac{1}{M}\sum_{i=1}^M \tilde{\mathcal{E}}_i^{l-1} \operatorname{var}[C_{im}^l]}, \tag{22}$$

where $\tilde{\mathcal{E}}_i^l = (1-(\rho_i^l)^2)\mathcal{E}_i$. Note that (8) is a special case of (22) provided we adopt the convention that $\rho_m^0 = 0$.

We next optimize the SNIR over the choice of equalizer, assuming sufficiently slow fading that in each pass l

$$C_{mi}^l(\omega;n) \approx A_m(\omega;n)\, B_i^l(\omega;n). \tag{23}$$

In this case, the functional form of the SNIR (22) is such that the results from [1] can be immediately exploited to obtain the optimum equalizer

$$B_m^l(\omega;n) \propto \frac{A_m^*(\omega;n)}{\mathcal{N}_0\mathcal{W}_0 + \frac{1}{M}\sum_i \tilde{\mathcal{E}}_i^{l-1} |A_i(\omega;n)|^2}. \tag{24}$$

To implement this equalizer, we require an algorithm for computing the correlation coefficients ρ_m^l. For this purpose, we write the output of the associated slicer as

$$e_m^l[n] = \hat{x}_m^l[n] - x_m[n], \tag{25}$$

and note that when $N > 2$ and $x_m[n] = \sqrt{\mathcal{E}_m}$, we have the approximation that $e_m^l[n]$ takes on the values $-2\sin^2(\pi/N) \pm j2\sin(\pi/N)\cos(\pi/N)$ each with probability $\Pr(\varepsilon_m^l)/2$ and takes on the value zero otherwise. Thus, exploiting symmetry,

$$\begin{aligned} E\left[x_m[n]\cdot e_m^l[n]\right] &= E\left[x_m[n]\cdot e_m^l[n] \,\middle|\, x_m[n] = \sqrt{\mathcal{E}_m}\right] \\ &= -2\sin^2\left(\frac{\pi}{N}\right)\mathcal{E}_m \Pr(\varepsilon_m^l). \end{aligned} \tag{26}$$

Finally, using (26) with (20), we obtain, for $l \geq 1$,

$$\rho_m^l = \frac{E\left[x_m[n]\, x_m[n]\right] + E\left[x_m[n]\, e_m^l[n]\right]}{\mathcal{E}_m}$$
$$\approx 1 - 2\sin^2\left(\frac{\pi}{N}\right) \mathcal{E}_m \Pr(\varepsilon_m^l). \tag{27}$$

Substituting (17) into (27) we see that we can recursively compute ρ_m^l given a convenient expression for mapping ρ_m^{l-1} to γ_m^l. In the sequel, we develop such mappings and analyze the performance of the algorithm.

IV. PERFORMANCE

We first consider forward link transmission, corresponding to the case in which all messages are transmitted through the same channel, i.e., $a_m[n;k] = a[n;k]$ for all m. With the optimal equalizer (24) in each pass of the mth receiver the SNIR after the lth pass (8) can be simplified to [8]

$$\gamma_m^{l+1} = \frac{1}{\zeta_m}\left(\frac{1}{e^{\xi^l} E_1(\xi^l)} - \xi^l\right), \tag{28}$$

where $1/\zeta_m = (\mathcal{E}_m \sigma_m^2)/(\mathcal{N}_0 \mathcal{W}_0)$ is the SNR at which the mth user's transmission is received, and where

$$\frac{1}{\xi^l} = \frac{1}{M}\sum_{i=1}^{M} \frac{1-(\rho_i^l)^2}{\zeta_i}, \tag{29}$$

with $E_1(\cdot)$ denoting the exponential integral $E_1(s) = \int_s^\infty e^{-t}/t\, dt$. Note that if $\rho_i^l \to 1$ for all i, then $\gamma_m^{l+1} \to 1/\zeta_m$, which substituted into (17) yields the performance of the AWGN channel.

The following algorithm predicts the performance of the multipass receiver as a function of the number of iterations used:

1. Set $\rho_m^0 = 0$ and let $l = 1$.
2. For each m, compute the SNIR γ_m^l at the slicer input on the lth decoding pass from the correlation ρ_m^{l-1} and channel SNR via (28) with (29). Then, from the slicer input SNIR γ_m^l, use (17) to compute the symbol error probability $\Pr(\varepsilon_m^l)$ at the slicer output.
3. Compute the normalized correlations ρ_m^l between the symbols $x_m[n]$ and the estimates $\hat{x}_m^l[n]$ produced at the slicer output via (27).
4. Increment l and go to step 2.

Although the algorithm applies more broadly, in the sequel we illustrate its key performance characteristics in the scenario in which power control is employed so that $\zeta_m = \zeta$ for all m. In this case, the optimum ρ_m^l are all identical as well, i.e., $\rho_m^l = \rho^l$ for all m.

For a given SNR $1/\zeta$, the relationship between ρ^{l-1} and $\Pr(\varepsilon^l)$ corresponding to Step 2 of the above procedure can be expressed in the form

$$\Pr(\varepsilon^l) = F(\zeta, \rho^{l-1}) \tag{30}$$

where the function $F(\cdot,\cdot)$ has the property that it is decreasing with both correlation ρ^l and SNR $1/\zeta$, as can be verified by substituting (28) into (17).

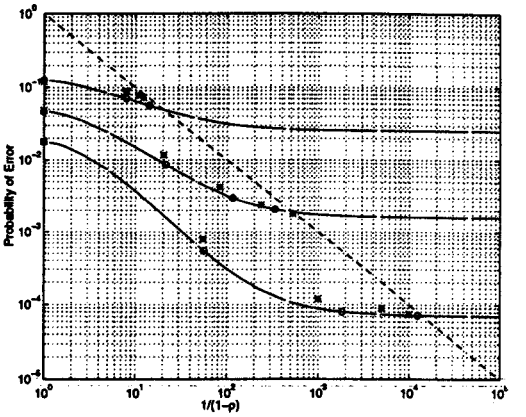

Fig. 4. Iterative receiver performance on the forward link. The successively lower solid curves plot QPSK symbol error rate as a function of the correlation coefficient ρ for SNRs of 7, 10, and 12 dB. Along each curve, o's identify the theoretically predicted decreasing error rates achieved with $l = 1, 2, \ldots$ decoding passes, and the intersections with the dashed line are the steady-state values ($l \to \infty$). The associated experimentally obtained values are depicted using $*$'s.

Since the mapping (27) of $\Pr(\varepsilon^l)$ to ρ^l in Step 3 is decreasing, it is straightforward to verify that ρ^l and hence $\Pr(\varepsilon^l)$ converge as $l \to \infty$. Moreover, substituting (30) into (27) with $l \to \infty$ we obtain that the steady-state correlation ρ^∞ is the unique solution to

$$1 - \rho^\infty = 2\sin^2\left(\frac{\pi}{N}\right) F(\zeta, \rho^\infty), \tag{31}$$

and that the steady-state symbol error rate is, in turn, $\Pr(\varepsilon^\infty) = F(\zeta, \rho^\infty)$.

These steady-state values are depicted in Fig. 4 for the case of QPSK ($N = 4$). In particular, the solid curves in the figure correspond to the right side of (31) plotted as a function of $1/(1-\rho)$ for several values of SNR $1/\zeta$, while the dashed line corresponds to a plot of the left side of (31). Hence, the intersections denote the steady-state values for the different SNR levels.

Fig. 4 also illustrates the predicted error rates as a function of iteration, which correspond to moving from the solid curves at $\rho = 0$ (iteration 1) horizontally to the dashed line, then vertically down to the solid curve (iteration 2), horizontally to the dashed line and down again to the solid curve (iteration 3), etc., in accordance with the algorithm described above. The results from Monte Carlo simulations involving 8 users with sufficiently long maximally-spread signatures are also shown, from which we can see the good accuracy of the theoretical predictions.

Note that as Fig. 4 reflects, the monotonicity properties of $F(\cdot,\cdot)$ ensure that the steady-state error rate $\Pr(\varepsilon^\infty)$ decreases monotonically with SNR. Moreover, the larger the SNR, the closer the correlation ρ^∞ is to unity, which as we discussed corresponds to the performance of the AWGN channel and therefore effectively perfect interference cancellation. These characteristics are illustrated more directly in Fig. 5, in which error rate is plotted as a function of SNR. This figure also suggests that comparatively few

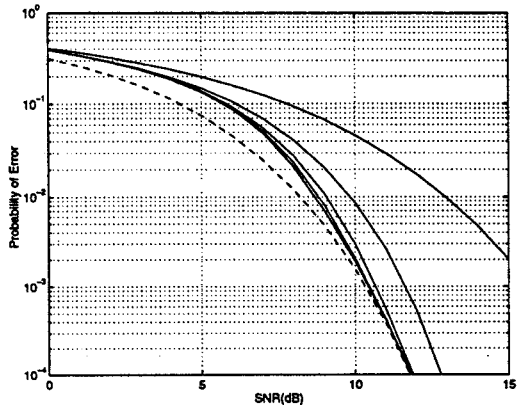

Fig. 5. Iterative receiver performance as a function of SNR on the forward link. The successively lower solid curves depict the symbol error rate as a function of SNR for 2,3,5, and ∞ decoding passes for QPSK transmission. The dashed curve is the corresponding AWGN channel performance.

(≤ 5) iterations of the decoding algorithm are required to converge to typical target bit error rates. This is significant since both the amount of computation and system delay are directly proportional to the number of iterations required.

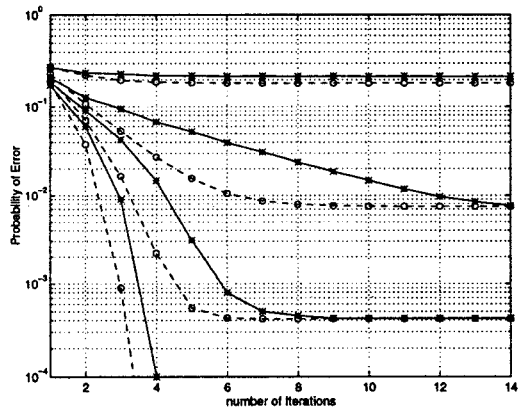

Fig. 6. Iterative receiver performance on the reverse link. The successively lower curves formed from o's connected by dashed lines depict predicted QPSK symbol error rate as a function of the number of decoding passes, for SNRs of 5,9,11, and 14 dB. The corresponding curves formed from $*$'s connected by solid lines are the experimental measurements.

Performance predictions can be obtained in a similar manner for reverse link scenarios. As an illustration, Fig. 6 depicts performance as a function of the number of decoding iterations with a simplified $M = 2$ user system employing power control. The corresponding plots of performance as a function of SNR are shown in Fig. 7. As these figures also reflect, a modest number of iterations generally suffices for convergence in this scenario as well. It is important to point out, however, that when large numbers of users are involved, the predictions tend to be somewhat overly optimistic even at high SNR. Such issues, as well as a number of others including sensitivity characteristics of

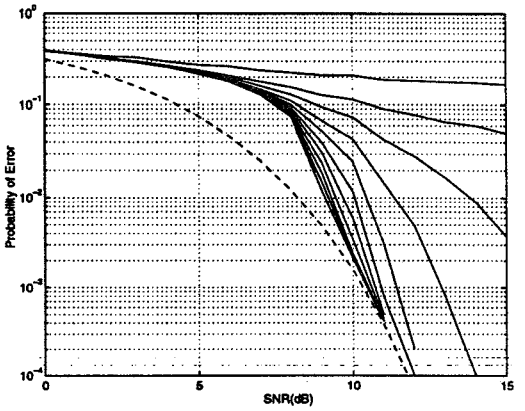

Fig. 7. Iterative receiver performance as a function of SNR on the reverse link. The successively lower solid curves depict the QPSK symbol error rate as a function of SNR for $1, 2, \ldots, 10$, and ∞ decoding passes. The dashed curve is the corresponding AWGN channel performance.

the iterative receiver, are explored in more detail in [8].

REFERENCES

[1] G. W. Wornell, "Spread-signature CDMA: Efficient multiuser communication in the presence of fading," *IEEE Trans. Inform. Theory*, vol. 41, pp. 1418–1438, Sept. 1995.

[2] G. W. Wornell, "Spread-response precoding for communication over fading channels," *IEEE Trans. Inform. Theory*, vol. 42, pp. 488–501, Mar. 1996.

[3] S. Verdú, "Minimum probability of error for asynchronous Gaussian multiple-access channels," *IEEE Trans. Inform. Theory*, vol. IT-32, pp. 85–96, Jan. 1986.

[4] G. D. Forney, Jr., "Maximum-likelihood sequence estimation of digital sequences in the presence of intersymbol interference," *IEEE Trans. Inform. Theory*, vol. IT-18, pp. 363–378, May 1972.

[5] A. Wittneben, "A novel bandwidth efficient analog coding/decoding scheme for data transmission over fading channels performance criteria," in *Proc. IEEE GLOBECOM*, 1994.

[6] J. G. Proakis, *Digital Communications*. New York, NY: McGraw-Hill, 2nd ed., 1989.

[7] J. M. Cioffi, G. P. Dudevoir, M. V. Eyuboglu, and G. D. Forney, Jr., "MMSE decision-feedback equalizers and coding—parts I and II," *IEEE Trans. Commun.*, vol. 43, pp. 2582–2604, Oct. 1995.

[8] S. Beheshti and G. W. Wornell, "Multipass receivers for spread-signature CDMA systems," 1997. Preprint, in preparation.